Dalton Transactions

RSC Publishing

PAPER

View Article Online
View Journal | View Issue

Microwave-assisted synthesis and up–down conversion luminescent properties of multicolor hydrophilic $LaF_3:Ln^{3+}$ nanocrystals†

Cite this: *Dalton Trans.*, 2013, **42**, 2015

Feifei Li,[a] Chunguang Li,[a] Xiaomin Liu,[b] Tianyu Bai,[a] Wenjun Dong,[c] Xiao Zhang,[a] Zhan Shi*[a] and Shouhua Feng[a]

Received 29th September 2012,
Accepted 30th October 2012

DOI: 10.1039/c2dt32295a

www.rsc.org/dalton

Monodisperse water-soluble $LaF_3:Ln^{3+}$ nanocrystals (NCs) have been successfully fabricated *via* a fast, facile and environmentally-friendly microwave-assisted modified polyol process with polyvinylpyrrolidone (PVP) as an amphiphilic surfactant. The obtained NCs can be well dispersed in hydrophilic solutions with small sizes in the range of 9–12 nm. The $LaF_3:Ln^{3+}$ NCs (Ln = Eu, Nd, Ce, Tb, Yb, Er, Yb, Ho and Yb, Tm) have the unique feature of up–down conversion from visible to NIR emission owing to the ladder-like arranged energy levels of Ln^{3+} and in particular, the high efficiency upconversion of the two-photon, obtained from excitation by a continuous 980 nm laser. This investigation focuses on both the up and down conversion fluorescence properties of water-soluble monodisperse crystalline $LaF_3:Ln^{3+}$ NCs in such a small size. Furthermore, the three-dimensional PDMS rod-like fluorescence displays and a silica surface modification by a core/shell structure on the obtained NCs can improve the biocompatibility, indicating potential applications in optical 3D devices and as bio-probes.

1. Introduction

In recent years, the synthesis and optical characterization of lanthanide-doped (Ln^{3+}-) fluoride NCs[1–9] have aroused material scientists' great interest due to their potential application in high-resolution displays, electroluminescent devices, lasers and optical telecommunication.[10] The luminescence of trivalent lanthanide ions is a result of transitions within the partially filled 4f shell of the ions, which are protected from the environment by the fully occupied 5s and 5p orbitals. These transitions are parity forbidden and in particular, the upconversion (UC) NCs exhibit anti-Stokes emission leading to a sharp emission bandwidth, long lifetime, tunable emission, high photostability and low cytotoxicity. The manipulation of the color output of UC nanomaterials has been widely used for biological labelling,[11] cancer treatment[12] and clinical applications.[13]

Lanthanum fluoride (LaF_3) NCs are an excellent host matrix for both UC and downconversion (DC) processes because of their adequate thermal and environmental stability, low phonon energy and ability to be easily doped with rare-earth ions.[14] In particular, Ln^{3+}-doped LaF_3 NCs have the unique feature of converting photons from the visible to the near infrared (NIR) region owing to the ladder-like arranged energy levels of Ln^{3+} and the high efficiency of the two-photon excitation obtained by continuous wave lasers. The amount of lanthanide ions doped into the NCs and the ratio between the different emitter ions can be varied to produce barcodes of fluorescent labels with different fluorescence emission spectra.[15,16] Therefore, the synthesis of Ln^{3+}-doped LaF_3 NCs has attracted considerable interest and various methods have recently been developed,[17–21] such as modified precipitation,[22] polyol[23] and solvothermal methods.[24] Van Veggel reported the synthesis of LaF_3 NCs in a mixed solvent composed of ethanol and water using NaF as the precipitator and citrate or phosphate monoester-based ligands.[25,26] Liu *et al.* have synthesized oil-soluble and hexagonally shaped Yb/Er, Yb/Tm and Yb/Ho codoped LaF_3 nanoplates through the decomposition of the respective $RE(TFA)_3$ in a multiphase system using a solvothermal technique.[17] By using KBF_4 as the fluoride source, $LaF_3:Eu^{3+}$ nanodisks with perfect crystallinity have been successfully synthesized through a facile and fast solution-based method

[a]*State Key Laboratory of Inorganic Synthesis and Preparative Chemistry, College of Chemistry, Jilin University, Changchun 130012, P. R. China. E-mail: zshi@mail.jlu.edu.cn; Fax: +86 431 85168624*
[b]*State Key Laboratory of Luminescence and Applications, Changchun Institute of Optics, Fine Mechanics and Physics, Chinese Academy of Sciences, Changchun 130033, P. R. China*
[c]*Center for Optoelectronics Materials and Devices, Department of Physics, Zhejiang Sci-Tech University, Hangzhou 310018, P. R. China*

†Electronic supplementary information (ESI) available: XPS, FT-IR spectrum, TG-DTA curve, solubility photos, emission spectra of $LaF_3:Ce^{3+}$, Tb^{3+} NCs, XRD and SEM of UC $LaF_3:Ln^{3+}$ NCs annealed at 600 °C, energy-transfer mechanisms of $LaF_3:Yb^{3+}$, Ho^{3+} NCs. See DOI: 10.1039/c2dt32295a

by Cao's group.[27] Zhang *et al.* have fabricated single-crystalline and monodisperse LaF_3 triangular and hexagonal nanoplates by thermolysis of $La(CF_3COO)_3$ in oleic acid/1-octadecene.[19] Up to now, the most effective and general method to prepare Ln^{3+}-doped LaF_3 nanoparticles with small sizes and good crystallinity has been the co-thermolysis of trifluoroacetate precursors at high temperature. Unfortunately, the hydrophobic NCs need further surface modification, which greatly affects their UC and DC luminescence and restricts their potential biological applications. In terms of *in vivo* biological applications, as is known to all, the prerequisites for an optimal universal bioprobe are water solubility, small sizes and high luminescence efficiency. Therefore, it is still a challenge to directly obtain water-soluble and biocompatible Ln^{3+}-doped LaF_3 with a small size and high UC and DC luminescence.

In this paper, we break through the above limitation by directly obtaining water-soluble, small sized and high UC–DC luminescent single-crystalline Ln^{3+}-doped LaF_3 NCs with PVP as the surfactant by a microwave-assisted approach. We have also achieved fine-tuning of the UC–DC emission, based on tuning the relative emission intensity of Ln^{3+}-doped LaF_3 NCs for color modulation from visible to NIR emission. PVP is an amphiphilic surfactant which can render the NCs dispersible in water and organic solvents.[28] Furthermore, its pyrrolidone groups can coordinate with lanthanide ions.[29] Moreover, a three-dimensional (3D) PDMS rod-like fluorescence application was researched and a thin silica surface was modified on the obtained NCs, indicating the optical 3D displays and potential bio-applications.

2. Experimental

2.1 Chemicals

High purity (99.9%) lanthanum chloride hydrate [$LaCl_3{\cdot}XH_2O$], europium chloride hexahydrate [$EuCl_3{\cdot}6H_2O$], terbium nitrate [$Tb(NO_3)_3{\cdot}6H_2O$], neodymium chloride hexahydrate [$NdCl_3{\cdot}6H_2O$], ytterbium chloride hexahydrate [$YbCl_3{\cdot}6H_2O$], erbium chloride hexahydrate [$ErCl_3{\cdot}6H_2O$], holmium chloride hexahydrate [$HoCl_3{\cdot}6H_2O$], thulium chloride hexahydrate [$TmCl_3{\cdot}6H_2O$], poly(vinylpyrrolidone) (PVP, M_w 30 000–40 000) and tetraethoxysilane (TEOS) were obtained from Sigma-Aldrich (Sigma-Aldrich, Singapore). Cerium nitrate [$Ce(NO_3)_3{\cdot}6H_2O$] (99%), ammonium fluoride NH_4F (96%), silicone elastomer prepolymer (Sylgard 184), curing agent and ethylene glycol (EG, 99%) were obtained from Sinopharm Chemical Reagent Co. Ltd. All the chemicals were used as obtained without further purification.

2.2 Synthesis of the nanocrystals

A commercial microwave reactor (ETHOS ONE, ITALY) system was used to perform the synthesis of the LaF_3:Ln^{3+} NCs. The preset profile (desired time and temperature) was followed automatically by continuously adjusting the applied microwave power. In a typical procedure, a 0.51 mmol portion of $LaCl_3{\cdot}XH_2O$, 0.072 mmol of $YbCl_3{\cdot}6H_2O$, 0.018 mmol of $ErCl_3{\cdot}6H_2O$ and 0.389 g of PVP were dissolved in 9 mL of EG at room temperature with stirring to form a homogeneous solution. Then, 1.8 mmol of NH_4F, dissolved in 6 mL of EG, was added drop wise to the reaction mixture. The mixture was transferred into the reacting vessel of the microwave reactor, heated to 200 °C for 8 min by microwave irradiation and then cooled to room temperature naturally. The product was isolated by centrifugation, washed with deionized water and ethanol in sequence and dispersed in 3 mL of ethanol. Other LaF_3:Ln^{3+} samples were prepared by a similar procedure except that $YbCl_3{\cdot}6H_2O$ and $ErCl_3{\cdot}6H_2O$ was replaced by the corresponding doped materials.

2.3 Synthesis of the 3D LaF_3:Ln^{3+} PDMS fluorescence displays

LaF_3:Ln^{3+} NCs were separated from the above ethanol solution (1.5 mL) and redispersed in EG (250 μL) by sonication. This EG solution was then mixed with a silicone elastomer prepolymer (4 g, Sylgard 184) and curing agent (0.75 g) with stirring and cross-linked in a rod mould at about 70 °C for 2 h.

2.4 Synthesis of the silica core-shell LaF_3:Ln^{3+} nanocrystals

PVP/LaF_3:Ln^{3+} NCs (0.05 mmol) were dispersed in ethanol (20 mL) and mixed with water (4 mL) and ammonia (30%, 0.5 mL). TEOS (0.06 mL), dissolved in ethanol (10 mL), was then added slowly to the solution with continuous stirring. The product was isolated by centrifugation and washed with water.

2.5 Characterization

XRD was performed on a Rigaku D/max-2500 diffractometer with a graphite monochromator using Cu–Kα radiation, operating at 200 mA and 40 kV. XRD data were collected over the range of 10–70° (2θ) with a step interval of 0.02° and a preset time of 1.6 s per step at room temperature. TEM and HRTEM images were recorded with a FEI Tecnai G2 S-Twin instrument with a field emission gun operating at 200 kV. All samples for TEM observation were prepared by dropping aqueous suspensions of uniformly dispersed nanoparticles onto carbon-coated copper grids. The IR spectra were acquired on a Bruker IFS 66v/S FTIR spectrometer. The surface of the manganese oxide nanocrystals was characterized by XPS data, which was collected on an ESCALAB 250 X-ray photoelectron spectroscopy, using Mg–Kα X-rays as the excitation source. Thermogravimetric experiments were performed with a TGA Q500 V20.10 Build 36 from room temperature to 800 °C at a heating rate of 10 °C min^{-1}. The emission and excitation spectra of the samples were recorded on an Edinburgh Instruments FLS920 spectrofluorimeter equipped with both continuous (450 W) and pulsed xenon lamps. La^{3+} life time values were measured using a nano second hydrogen flash lamp operating at 40 K H_2.

3. Results and discussion

3.1 Crystallinity, structures, morphology and surfactant analysis of the nanocrystals

The combination of a polyol system and microwave dielectric heating,[30–32] which has the advantages of higher heating rates, uniform heating without thermal gradients, selective heating properties and higher yields in shorter reaction times, could provide a facile and green route to fabricate nanomaterials. Here, crystallized LaF_3:Ln^{3+} NCs were successfully synthesized through a microwave-assisted polyol process. Ethylene glycol (EG) was chosen as the solvent because it could easily dissolve a variety of polar inorganic materials due to its high permittivity (ε = 32). As one can see from the XRD patterns (Fig. 1), a pure hexagonal phase structure of small LaF_3:Ln^{3+} NCs was obtained, which is consistent with the PDF standard card No. 32-0483 reported earlier. The broadening of the diffraction peaks indicates that the sizes of the doped LaF_3 NCs synthesized by our approach are at the nanoscale. The major (111), (302) and (221) peaks were used to calculate the average crystallite size of these NCs, which is about 11 nm, according to the Scherrer equation, $D = 0.90\lambda/\beta\cos\theta$.

Similar results which show a narrow size distribution were further obtained from the Transmission Electron Microscopy (TEM) images. Moreover, high crystallinity is important for phosphors because high crystallinity generally means fewer traps and stronger UC and DC luminescence.[33] In addition, X-ray photoelectron spectroscopy (XPS) was used to further confirm the composition and oxidation state of the as-prepared products (Fig. S1, ESI†). From the XPS analysis, we have determined that the oxidation states of the multivalent lanthanides, such as Eu; Nd; Ce, Tb; Yb, Er; Yb, Ho and Yb, Tm are trivalent for the as-obtained Ln^{3+}-doped LaF_3 up–down conversion nanocrystals.

The TEM images in Fig. 2 and 3 reveal the single-crystalline and monodisperse hexagonal DC and UC LaF_3:Ln^{3+} NCs, taking the DC LaF_3:Ce^{3+}, Tb^{3+} NCs and UC LaF_3:Yb^{3+}, Er^{3+} NCs as examples, respectively. The low-resolution transmission electron microscopy images clearly show very uniform DC (Fig. 2a and b) and UC (Fig. 3) LaF_3:Ln^{3+} NCs, with an average diameter of about 11 nm. Fig. 2c is the high-resolution transmission (HRTEM) image of an individual spherical LaF_3:Ce^{3+}, Tb^{3+} nanoparticle. The HRTEM image displays high crystallinity for the LaF_3:Ce^{3+}, Tb^{3+} NCs. The distance between the

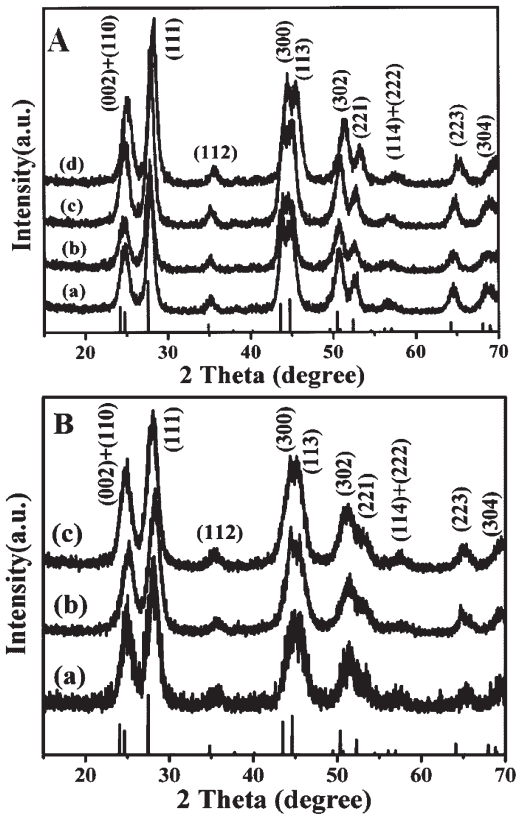

Fig. 1 The XRD pattern of the as-synthesized (A) DC LaF_3:Ln^{3+} NCs: (a) LaF_3; (b) LaF_3:Nd^{3+}; (c) LaF_3:Ce^{3+}, Tb^{3+}; (d) LaF_3:Eu^{3+}; (B) UC LaF_3:Ln^{3+} NCs: (a) LaF_3:Yb^{3+}, Tm^{3+}; (b) LaF_3:Yb^{3+}, Er^{3+}; (c) LaF_3:Yb^{3+}, Ho^{3+}. Literature values for the peak positions and intensities for the hexagonal LaF_3:Ln^{3+} NCs are indicated by the vertical bars.

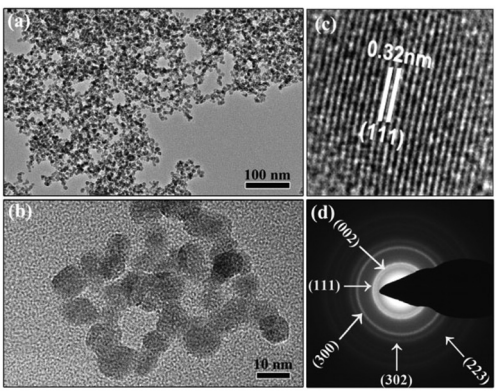

Fig. 2 (a, b) TEM images of the DC LaF_3:Ce^{3+}, Tb^{3+} NCs. (c) Typical HRTEM image of a DC LaF_3:Ce^{3+}, Tb^{3+} NC. (d) SAED patterns of the low-resolution LaF_3:Ce^{3+}, Tb^{3+} NCs.

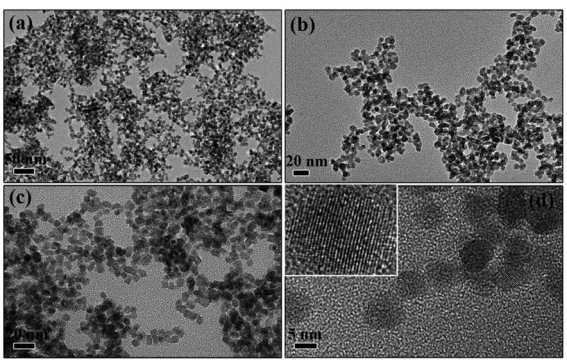

Fig. 3 (a, b, c) TEM images of the UC LaF_3:Yb^{3+}, Er^{3+} NCs. (d) Typical HRTEM image of a UC LaF_3:Yb^{3+}, Er^{3+} NC.

adjacent atomic lattice fringe is about 0.32 nm, which is consistent with the (111) planes of hexagonal LaF_3:Ce^{3+}, Tb^{3+} NCs. Both the HRTEM image and the selected area electron diffraction (SAED) (Fig. 2c and d) patterns reveal the nanocrystalline nature of the samples, which further confirms that the particle features high crystallinity, contributing to the strong UC and DC luminescence. Therefore, we have directly synthesized water-soluble and high up–down conversion hexagonal phase Ln^{3+}-doped LaF_3 NCs *via* an environmentally-friendly microwave-assisted route with small sizes and good dispersibility.

In the synthesis, we used PVP as a chelating agent and stabilizer. In the FT-IR spectra (Fig. S2, ESI†), both the pure PVP and the PVP-coated LaF_3:Ln^{3+} NCs clearly show additional bands centered at about 2953 and 2885 cm^{-1}, which can be assigned to the CH_2 stretching modes of PVP: $\nu_{as}(CH_2)$ for the pyrrolidone ring and $\nu_{as}(CH_2)$ for the polymer backbone, respectively. Consistent with previous observations, the C=O stretching band of PVP, originally at ~1678 cm^{-1}, shifts to a lower frequency of ~1653 cm^{-1} upon forming a hydrogen bond with the sample's surface, which confirms that PVP is coordinated with the lanthanide ions.[34]

Further proof is given in Fig. S3 in the ESI.† As the temperature increases there is an obvious weightlessness of 12.55% in the TG-DTA curve of LaF_3:Yb^{3+}, Er^{3+} NCs. Therefore, the Ln^{3+} ions are complexed with the pyrrolidone groups of PVP and then react with F^- in the viscous and weakly polar solvent EG and thus small NCs are formed. As a result of the good solubility of PVP in water and many organic solvents, it is expected that the PVP/LaF_3:Ln^{3+} NCs can be well dispersed in water and many organic solvents to form colloidal solutions. The photograph in Fig. S4 in the ESI† demonstrates that the PVP, capped on the LaF_3:Ln^{3+} NCs, can be well-dispersed in various solvents including water, methanol, ethanol, EG, chloroform, dimethylformamide and dimethylsulfoxide, to obtain a nearly transparent solution. As a result, PVP can not only help to control the nucleation and growth of the crystals but also render the LaF_3:Ln^{3+} NCs water-soluble.

3.2 Downconversion photoluminescence properties

Doping of the LaF_3 host with selected luminescent Ln^{3+} ions allows these NCs to display a range of emission lines from the visible to the near-infrared region (λ = 450–1650 nm). These results reveal that these NCs have potential applications as fluorescent labels for biomolecules.[35] Therefore, the up–down conversion luminescent properties of different lanthanide-doped LaF_3 NCs in an aqueous solution were carefully investigated in this work. Fig. 4a shows the luminescent spectra of LaF_3:45% Ce^{3+}, 15% Tb^{3+} NCs and the inset shows the strong green emission under exposure to the 264 nm UV light. The excitation spectrum is monitored with the 542 nm emission ($^5D_4$–$^7F_5$) of Tb^{3+}, corresponding to the absorption of the 4f–5d band of Ce^{3+}. The weak emission of Ce^{3+} (280–400 nm) and the typically strong emission of Tb^{3+} (400–750 nm) (Fig. S5, ESI†), due to transitions between the excited $^5D_4$ state and the ^7F_J (J = 6–3) ground states of the Tb^{3+} ions, are also observed for an energy transfer from Ce^{3+} to Tb^{3+}.[36] The quantum yield was

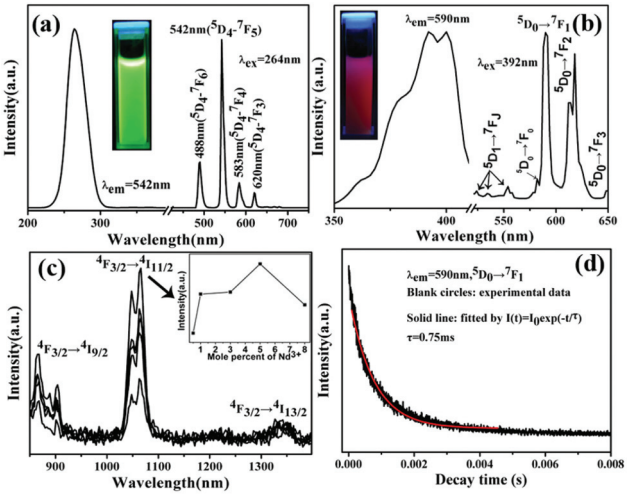

Fig. 4 Fluorescence spectra of the DC LaF_3:Ln^{3+} NCs. (a) Excitation (left) and emission (right) spectra of the LaF_3:Ce^{3+}, Tb^{3+} NCs. (b) Excitation (left) and emission (right) spectra of the LaF_3:Eu^{3+} NCs. (c) Emission spectra of the LaF_3:Nd^{3+} NCs. (d) Decay curve of the Eu^{3+} luminescence in the LaF_3:Eu^{3+} NCs. The insets show: (a, b) the corresponding luminescence photographs of the samples under a UV lamp. (c) The effect of Nd^{3+} concentration (x) on the emission intensity of the LaF_3:Nd^{3+} NCs.

calculated from the equation $Y_{sam} = Y_{sta}$ $(I_{sam}A_{sta}/I_{sta}A_{sam})$, in which A is the absorption intensity and I is the integral fluorescence intensity. The quantum yield of quinine bisulfate is 54.6%. By measuring the luminescence of both Ce^{3+} and Tb^{3+} and LaF_3:Ce^{3+}, Tb^{3+} NCs dispersed in water, a quantum yield of 18% was obtained.

Meanwhile, the room temperature excitation (λ_{em} = 590 nm) and emission (λ_{ex} = 392 nm) spectra of the LaF_3:5% Eu^{3+} NCs are shown in Fig. 4b. We can clearly see in the excitation spectrum, the characteristic absorption bands of Eu^{3+}, in which the most intense peak at λ = 392 nm corresponds to the $^7F_0$–$^5L_6$ transition of Eu^{3+}. The major emission bands of Eu^{3+} at λ = 590 and 618 nm are assigned to the $^5D_0$–$^7F_1$ and $^5D_0$–$^7F_2$ transitions. Therefore, the emission spectrum is mainly located in the red spectral area, as shown in the inset of Fig. 4b. The photoluminescence decay curves and lifetime of Eu^{3+} ($^5D_0$–$^7F_1$, 590 nm) in the LaF_3:Eu^{3+} NCs are shown in Fig. 4d. All these curves can be fitted into a single exponential function as $I = I_0 \exp(-t/\tau)$, and the lifetime of Eu^{3+} is determined to be 0.75 ms.

Additionally, Nd^{3+} doped nanomaterials have a variety of applications in optical telecommunication windows and for polymer-based optical components due to their near infrared emissions. LaF_3:Nd^{3+} NCs can be excited at 800 nm. The emission peaks at 880, 1053 and 1330 nm correspond to the transitions from $^4F_{3/2}$ to $^4I_{9/2}$, $^4I_{11/2}$ and $^4I_{13/2}$, as shown in Fig. 4c, respectively. The $^4F_{3/2} \rightarrow {}^4I_{11/2}$ transition is a typical magnetic dipole transition, generally investigated and applied in the near-IR region. By comparing the emission spectra of the as prepared Nd^{3+}-doped LaF_3 NCs with Nd^{3+} concentrations from 0.5 to 8 mol%, we produce a fluorescent intensity change curve. The emission spectra of the LaF_3:Nd^{3+} NCs with

different Nd^{3+} doped concentrations were obtained using the same fluorescence spectroscopy testing conditions. As the concentration is increased, the fluorescence intensity reaches a maximum at 5 mol%. When the Nd^{3+} concentration is further increased, concentration quenching happens and the intensity is decreased (Fig. 4c inset). This is because the average distance among the Nd^{3+} ions is so large at low concentration that the energy transfer interaction is very weak. Thus, concentration quenching does not occur. When the concentration increases above 5 mol%, the nonradiative energy transfer interaction between nearby rare-earth ions is stronger. Therefore, concentration quenching occurs and the intensity is decreased. The LaF_3 NCs doped with Nd^{3+} are a promising material for polymer-based optical components because they show luminescence in the telecommunication window.

3.3 Upconversion photoluminescence properties and luminescence mechanism

LaF_3 has been considered an ideal host lattice for optically active Ln^{3+} and different doping modes may lead to quite different emission behaviors, which promise applications such as biological labeling. In addition to the DC luminescence properties, we have also further investigated the UC properties. Fig. 5a–c show the UC fluorescence spectra of the LaF_3:12% Yb^{3+}, 3% Er^{3+}, LaF_3:20% Yb^{3+}, 2% Tm^{3+} and LaF_3:20% Yb^{3+}, 1% Ho^{3+} NCs, respectively. For the Er^{3+}-doped NCs, there are three emission peaks at 530, 540 and 656 nm, which are assigned to the $^4H_{11/2}$–$^4I_{15/2}$, $^4S_{3/2}$–$^4I_{15/2}$, and $^4F_{9/2}$–$^4I_{15/2}$ transitions of Er^{3+}, respectively. For the Tm^{3+}-doped NCs, the blue emission bands are assigned to the $^1D_2$–$^3F_4$, and $^1G_4$–$^3H_6$ transitions, while the red emission is assigned to the $^1G_4$–$^3F_4$ transition. For the NCs doped with Ho^{3+}, the emission at 642 nm is assigned to the $^5F_5$–$^5I_8$ transition and the green emission at 540 nm corresponds to the $^5S_2$–$^5I_8$ transition. Up to now, there have been few reports on the water-soluble LaF_3:Yb^{3+}, Ln^{3+} upconversion NCs which have visible UC luminescence with small sizes. In order to obtain strong upconversion emission, we treated the LaF_3:Yb^{3+}, Ln^{3+} UC NCs. When the samples were annealed at a temperature of 600 °C, the corresponding sharp UC fluorescence enhancement was observably increased for the LaF_3:Ln^{3+} NCs. The annealed samples can be easily redispersed in ethanol and show strong UC luminescence intensity when excited by a 980 nm laser and we can see the corresponding colour in the inset of Fig. 5a–c. Fig. S6 and S7 in the ESI† show the annealed samples' structure and morphology, respectively. It is also worth mentioning the lifetime of one of the typical dopings. As mentioned, here we take the annealed LaF_3:12%Yb^{3+}, 3%Er^{3+} UC NCs as examples to show the UC NCs' lifetime. The LaF_3:Yb^{3+}, Er^{3+} NCs' dynamic emission data for the $^4S_{3/2}$–$^4I_{15/2}$ transition of Er^{3+} is 0.31 ms, as shown in Fig. 5d. The above results demonstrates that these UC fluorescent LaF_3:Yb^{3+}, Ln^{3+} NCs have good upconversion emission intensity and would have potential applications in many fields such as solid-state lasers, lighting and displays, *etc*.

To investigate the UC luminescence mechanism, the power dependence of the luminescence intensity is monitored (Fig. 6a). As is well known, the emission intensity, I_{UC}, is proportional to the excitation intensity, I_{IR}: $I_{UC} \propto I_{IR}^{n}$,[37] where n is the number of pump photons involved in the UC process, as determined from the slope of a logarithmic plot of the UC intensity *vs.* the pump power. Thus, the power dependent UC

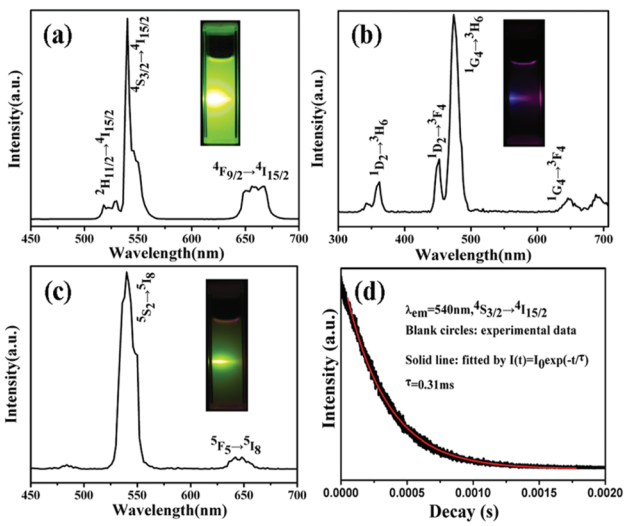

Fig. 5 Fluorescence spectra of the UC NCs (a) LaF_3:Yb^{3+}, Er^{3+}; (b) LaF_3:Yb^{3+}, Tm^{3+}; (c) LaF_3:Yb^{3+}, Ho^{3+} NCs; The insets show: (a, b, c) the corresponding UC luminescence photographs of the annealed samples under a 980 nm laser; (d) Decay curve of the Er^{3+} luminescence (λ_{em} = 540 nm) in the annealed LaF_3:Yb^{3+}, Er^{3+} NCs under 980 nm NIR excitation.

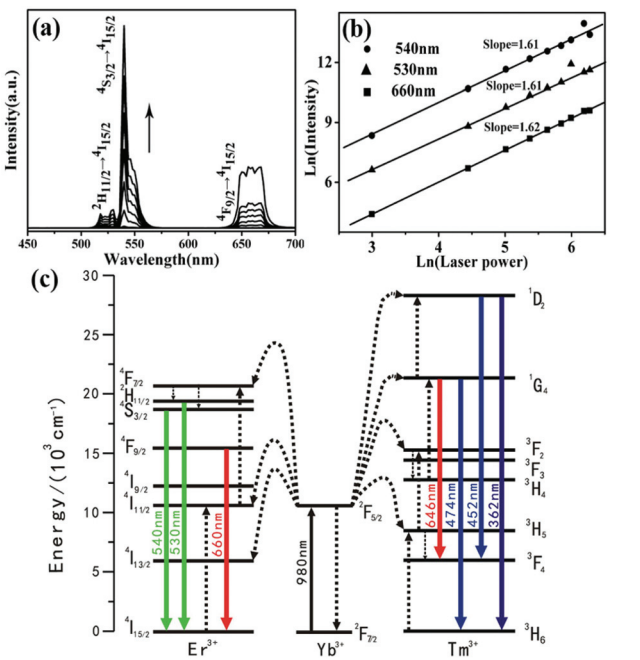

Fig. 6 (a, b) Dependences of the UC luminescence on the CW excitation intensity of 980 nm for the LaF_3:Yb^{3+}, Er^{3+} NCs. (c) Proposed energy-transfer mechanisms showing the UC processing Er^{3+}, Tm^{3+}, and Yb^{3+} doped NCs under 980 nm laser diode excitation.

spectra were recorded to determine the number of photons responsible for the UC process (Fig. 6b). The slopes for the red and green emissions are approximately equal to two, indicating two incident NIR photons are needed for each emitted photon. With prominent two-photon absorption and subsequent energy transfer, LaF_3:Yb^{3+}, Er^{3+} emitters possess a unique UC luminescence which is not susceptible to the outer environment as a result of the 4f-intraconfigurational transitions. Moreover, we take the LaF_3:Yb^{3+}, Er^{3+}/Tm^{3+} NCs as examples to indicate the two-photon mechanism of the fluorescence resonance energy transfer, as shown in Fig. 6c. In addition, the energy-transfer mechanisms of the LaF_3:Yb^{3+}, Ho^{3+} NCs are shown in Fig. S8 in the ESI.† First, an initial energy transfer from a Yb^{3+} ion in the $^2F_{5/2}$ state to an Er^{3+} ion populates the $^4I_{11/2}$ level and then moves to the $^4F_{7/2}$ level by absorbing the energy of another excited Yb^{3+} ion or another 980 nm photon. The Er^{3+} ion can then relax non-radiatively to the $^2H_{11/2}$ and $^4S_{3/2}$ levels and the green $^2H_{11/2}$–$^4I_{15/2}$ and $^4S_{3/2}$–$^4I_{15/2}$ emissions occur. Alternatively, the ion can further relax and populate the $^4F_{9/2}$ level, leading to the red $^4F_{9/2}$–$^4I_{15/2}$ emission. The $^4F_{9/2}$ level may also be populated from the $^4I_{13/2}$ level of the Er^{3+} ion by the absorption of a 980 nm photon or energy transfer from another Yb^{3+} ion. Meanwhile, there are four subsequent energy transfers from Yb^{3+} to populate the upper Tm^{3+} levels and various emissions can occur for the LaF_3:Yb^{3+}, Tm^{3+} NCs.

3.4 PDMS solid nanocomposites and LaF_3:Ln^{3+}@SiO_2 core-shell structures

Owing to their small feature size and ease of dispersion, these annealed LaF_3:Ln^{3+} NCs can readily be incorporated in polydimethylsiloxane (PDMS) monoliths to construct volumetric 3D rod-like colour displays, presenting unique interface applications for 3D image visualization. The fabrication of solid composite materials is briefly illustrated in Fig. 7a. The LaF_3:Eu^{3+} NCs were redispersed in an EG solution after being separated from ethanol because EG solutions form very stable droplets in the liquid prepolymer of PDMS.[38] The prepolymer, containing liquid droplets of the LaF_3:Eu^{3+} NCs dispersion, was then solidified to form a composite rod through polymerization when an external 392 nm UV light was exposed to the PDMS rod as the LaF_3:Eu^{3+} NCs are still able to assemble into each droplet, which can diffract light in the same wavelength and therefore collectively display a sharp red colour which can be obviously perceived. Fig. 7b demonstrates a stable and flexible 3D composite rod with UV light or 980 nm laser responsive optical properties. The excitation light was chosen according to different dopant Ln^{3+} ions. As schematically illustrated in Fig. 7c, a simple display unit has been demonstrated by fabricating a patterned PDMS film with LaF_3:Ce^{3+}, Tb^{3+} NCs and without LaF_3:Ce^{3+}, Tb^{3+} NCs for the letters and background, respectively. Without an external light, the film shows the native gray colour of the LaF_3:Ce^{3+}, Tb^{3+} NCs with essentially no contrast except for the small amount of roughness at the edges of the letters resulting from the templating process. With irradiation with a 264 nm UV light however, bright green letters with a striking contrast against the gray background can be clearly observed (Fig. 7d).

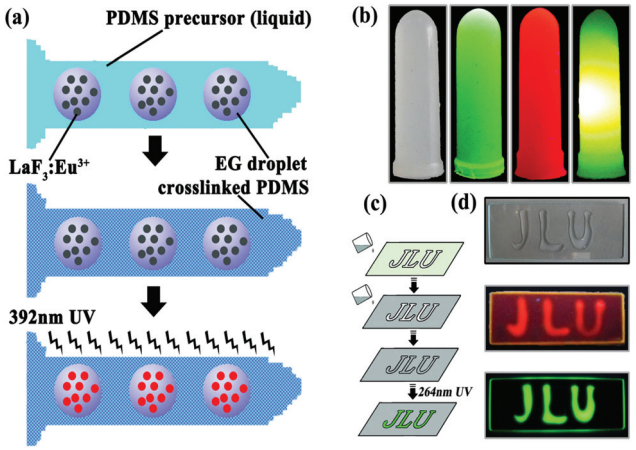

Fig. 7 (a) Schematic illustration showing the fabrication procedure for a UV light-responsive PDMS composite embedded with EG droplets containing LaF_3:Eu^{3+} NCs. (b) LaF_3:Ln^{3+} NCs (Ce^{3+}, Tb^{3+}, Eu^{3+}, Yb^{3+}, Er^{3+}) with the corresponding excited light induced color change of the PDMS rod. (c) Schematic illustration of the two-step procedure for fabricating a patterned composite PDMS film. (d) Digital photos of a patterned PDMS film that displays letters upon the application of an external UV light.

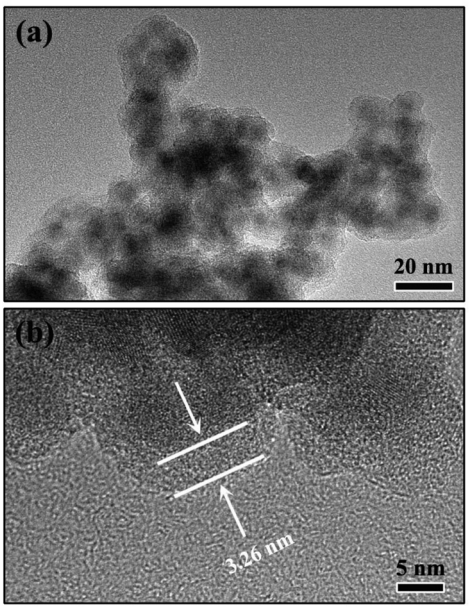

Fig. 8 (a) TEM image of silica-coated PVP/LaF_3:Yb^{3+}, Er^{3+} NCs. (b) HRTEM image of PVP/LaF_3:Yb^{3+}, Er^{3+} NCs@SiO_2.

Moreover, a thin layer of silica is coated onto the PVP/LaF_3:Ln^{3+} NCs to form a core/shell structure (Fig. 8) and the silica thickness can be adjusted to 3 nm. The surface modified core/shell structure on the obtained PVP/LaF_3:Ln^{3+} NCs can improve the biocompatibility, which fully indicates these UC and DC NCs have great potential for biological applications as new fluorescent labeling nanomaterials.

4. Conclusions

In summary, we have successfully synthesized water-soluble LaF_3:Ln^{3+} up–down conversion fluorescent colloidal NCs by a microwave-assisted polyol method. The ultra small size of the NCs is in the range of 9–12 nm. Surface-tethered PVP polymer chains render the particles highly water-dispersible. By changing the doped rare-earth ions, we present a series of color modulation from visible to NIR emission. Moreover, we utilise the fluorescent properties for 3D PDMS rod-like displays and a thin silica core/shell structure which can improve the biocompatibility. The results suggest that these up–down conversion NCs have great potential as optical 3D devices and biological fluorescent labeling nanomaterials.

Acknowledgements

This work was supported by the Foundation of the National Natural Science Foundation of China (No. 20971054, 90922034 and 21131002), the Specialized Research Fund for the Doctoral Program of Higher Education (No. 20110061110015), the Postdoctoral Science Foundation of China (No. 20110491294) and the Zhejiang Provincial Natural Science Foundation of China (LR12E02001).

Notes and references

1 (*a*) X. Wang, J. Zhuang, Q. Peng and Y. D. Li, *Nature*, 2005, **437**, 121; (*b*) J.-C. Boyer, C.-J. Carling, B. D. Gates and N. R. Branda, *J. Am. Chem. Soc.*, 2010, **132**, 15766; (*c*) D. T. Tu, L. Q. Liu, Q. Ju, Y. S. Liu, H. M. Zhu, R. F. Li and X. Y. Chen, *Angew. Chem., Int. Ed.*, 2011, **50**, 6306; (*d*) Q. Ju, D. T. Tu, Y. S. Liu, R. F. Li, H. M. Zhu, J. C. Chen, Z. Chen, M. D. Huang and X. Y. Chen, *J. Am. Chem. Soc.*, 2012, **134**, 1323.

2 (*a*) F. Wang, Y. Han, C. S. Lim, Y. H. Lu, J. Wang, J. Xu, H. Y. Chen, C. Zhang, M. H. Hong and X. G. Liu, *Nature*, 2010, **463**, 1061; (*b*) J. N. Liu, W. B. Bu, S. J. Zhang, F. Chen, H. Y. Xing, L. M. Pan, L. P. Zhou, W. J. Peng and J. L. Shi, *Chem.–Eur. J.*, 2012, **18**, 2335; (*c*) H. Hu, L. Q. Xiong, J. Zhou, F. Y. Li, T. Y. Cao and C. H. Huang, *Chem.–Eur. J.*, 2009, **15**, 3577.

3 (*a*) F. Wang and X. G. Liu, *J. Am. Chem. Soc.*, 2008, **130**, 5642; (*b*) F. Zhang, J. Li, J. Shan, L. Xu and D. Y. Zhao, *Chem.–Eur. J.*, 2009, **15**, 11010; (*c*) C. G. Li, F. F. Li, T. Li, T. Y. Bai, L. Wang, Z. Shi and S. H. Feng, *Dalton Trans.*, 2012, **41**, 4890.

4 (*a*) W. Feng, L. D. Sun, Y. W. Zhang and C. H. Yan, *Small*, 2009, **18**, 2057; (*b*) N. Bogdan, F. Vetrone, G. A. Ozin and J. A. Capobianco, *Nano Lett.*, 2011, **11**, 835.

5 (*a*) Y. S. Liu, D. T. Tu, H. M. Zhu, R. F. Li, W. Q. Luo and X. Y. Chen, *Adv. Mater.*, 2010, **22**, 3266; (*b*) H. T. Wong, F. Vetrone, R. Naccache, H. L. W. Chan, J. H. Hao and J. A. Capobianco, *J. Mater. Chem.*, 2011, **21**, 16589.

6 L. H. Fischer, G. S. Harms and O. S. Wolfbeis, *Angew. Chem., Int. Ed.*, 2011, **50**, 4546.

7 J. C. Boyer, L. A. Cuccia and J. A. Capobianco, *Nano Lett.*, 2007, **7**, 847.

8 F. F. Li, C. G. Li, X. M. Liu, Y. Chen, T. Y. Bai, L. Wang, Z. Shi and S. H. Feng, *Chem.–Eur. J.*, 2012, **18**, 11641.

9 D. K. Chatterjee, M. K. Gnanasammandhan and Y. Zhang, *Small*, 2010, **6**, 2781.

10 (*a*) D. B. Barber, C. R. Pollock, L. L. Beecroft and C. K. Ober, *Opt. Lett.*, 1997, **22**, 1247; (*b*) W. Wu, L. M. Yao, T. S. Yang, R. Y. Yin, F. Y. Li and Y. L. Yu, *J. Am. Chem. Soc.*, 2011, **133**, 15810.

11 (*a*) G. S. Yi and G. M. Chow, *J. Mater. Chem.*, 2005, **15**, 4460; (*b*) R. Kumar, M. Nyk, T. Y. Ohulchanskyy, C. A. Flask and P. N. Prasad, *Adv. Funct. Mater.*, 2009, **19**, 853; (*c*) F. Wang, D. Banerjee, Y. S. Liu, X. Y. Chen and X. G. Liu, *Analyst*, 2010, **135**, 1839; (*d*) J. Zhou, M. X. Yu, Y. Sun, X. Z. Zhang, X. J. Zhu, Z. H. Wu, D. M. Wu and F. Y. Li, *Biomaterials*, 2011, **32**, 1148.

12 (*a*) P. Zhang, W. Steelant, M. Kumar and M. Scholfield, *J. Am. Chem. Soc.*, 2007, **129**, 4526; (*b*) M. He, P. Huang, C. L. Zhang, H. Y. Hu, C. C. Bao, G. Gao, R. He and D. X. Cui, *Adv. Funct. Mater.*, 2011, **21**, 4470.

13 (*a*) G. S. Yi, H. C. Lu, S. Y. Zhao, Y. Ge, W. J. Yang, D. P. Chen and L. H. Guo, *Nano Lett.*, 2004, **4**, 2191; (*b*) F. Meiser, C. Cortez and F. Caruso, *Angew. Chem., Int. Ed.*, 2004, **43**, 5954.

14 R. F. Qin, H. W. Song, G. H. Pan, X. Bai, B. Dong, S. H. Xie, L. Liu, Q. L. Dai, X. S. Qu, X. G. Ren and H. F. Zhao, *Cryst. Growth Des.*, 2009, **9**, 1750.

15 F. Auzel, *Chem. Rev.*, 2004, **104**, 139.

16 T. Soukka, K. Kuningas, T. Rantanen, V. Haaslahti and T. Lövgren, *J. Fluoresc.*, 2005, **15**, 513.

17 C. H. Liu and D. P. Chen, *J. Mater. Chem.*, 2007, **17**, 3875.

18 F. Wang, Y. Zhang, X. P. Fan and M. Q. Wang, *J. Mater. Chem.*, 2006, **16**, 1031.

19 Y. W. Zhang, X. Sun, R. Si, L. P. You and C. H. Yan, *J. Am. Chem. Soc.*, 2005, **127**, 3260.

20 J. S. Zhang, W. P. Qin, D. Zhao, G. J. H. Dea, J. S. Zhang, Y. Wang and C. Y. Cao, *J. Lumin.*, 2006, **119–120**, 341.

21 H. Hu, Z. G. Chen, T. Y. Cao, Q. Zhang, M. X. Yu, F. Y. Li, T. Yi and C. H. Huang, *Nanotechnology*, 2008, **19**, 375702.

22 J. W. Stouwdam and F. C. J. M. van Veggel, *Nano Lett.*, 2002, **2**, 733.

23 Y. Wei, F. Q. Lu, X. R. Zhang and D. P. Chen, *Mater. Lett.*, 2007, **61**, 1337.

24 L. Y. Wang and Y. D. Li, *Chem.–Eur. J.*, 2007, **13**, 4203.

25 S. Sivakumar, F. C. J. M. van Veggel and M. Raudsepp, *J. Am. Chem. Soc.*, 2005, **127**, 12464.

26 P. R. Diamente, R. D. Burke and F. C. J. M. van Veggel, *Langmuir*, 2006, **22**, 1782.

27 L. Zhu, J. Meng and X. Q. Cao, *Eur. J. Inorg. Chem.*, 2007, **24**, 3863.

28 Z. Q. Li and Y. Zhang, *Angew. Chem., Int. Ed.*, 2006, **45**, 7732.

29 Q. Li, T. Li and J. G. Wu, *J. Phys. Chem. B*, 2001, **105**, 12293.

30 (*a*) X. L. Hu and J. C. Yu, *Adv. Funct. Mater.*, 2008, **18**, 880; (*b*) H. Q. Wang and T. Nann, *ACS Nano*, 2009, **3**, 3804.
31 C. Chen, L. D. Sun, Z. X. Li, L. L. Li, J. Zhang, Y. W. Zhang and C. H. Yan, *Langmuir*, 2010, **26**, 8797.
32 C. X. Li, P. A. Ma, P. P. Yang, Z. H. Xu, G. G. Li, D. M. Yang, C. Peng and J. Lin, *CrystEngComm*, 2011, **13**, 1003.
33 X. C. Jiang, L. D. Sun, W. Feng and C. H. Yan, *Cryst. Growth Des.*, 2004, **4**, 517.
34 Q. Zhang, T. R. Zhang, J. P. Ge and Y. D. Yin, *Nano Lett.*, 2008, **8**, 2867.
35 S. Sivakumar, F. C. J. M. van Veggel and P. S. May, *J. Am. Chem. Soc.*, 2007, **129**, 620.
36 X. X. Zhu, Q. H. Zhang, Y. G. Li and H. Z. Wang, *J. Mater. Chem.*, 2008, **18**, 5060.
37 C. H. Li, X. F. Yang, J. C. Yu, T. Ming and J. F. Wang, *Chem. Commun.*, 2011, **47**, 3511.
38 (*a*) C. G. Li, T. Y. Bai, T. Li, F. F. Li, W. J. Dong, Z. Shi and S. H. Feng, *Eur. J. Inorg. Chem.*, 2012, **8**, 1204; (*b*) G. J. Ping and Y. D. Yin, *Adv. Mater.*, 2008, **20**, 3485.

